Extinction and coexistence in a binary mixture of proliferating motile disks

Alejandro Almodóvar,* Tobias Galla,† and Cristóbal López‡
IFISC, Instituto de Física Interdisciplinar y Sistemas Complejos (CSIC-UIB), Campus Universitat de les Illes Balears, E-07122 Palma de Mallorca, Spain

(Received 29 January 2024; accepted 16 May 2024; published 18 June 2024)

A binary mixture of two-different-size proliferating motile disks is studied. As growth is space limited, we focus on the conditions such that there is a coexistence of both large and small disks, or dominance of the larger disks. The study involves systematically varying some system parameters, such as diffusivities, growth rates, and self-propulsion velocities. In particular, we demonstrate that diffusing faster confers a competitive advantage, so that larger disks can in the long time coexist or even dominate the smaller ones. In the case of self-propelled disks, a coexistence regime is induced by the activity where the two types of disks show the same spatial distribution: both particles are phase separated or both are homogeneously distributed in the whole system.

DOI: 10.1103/PhysRevE.109.064140

I. INTRODUCTION

Motivated by the collective dynamics in biological phenomena such as wound healing [1–3], tissue formation [4], the expansion of tumors [5], or the dynamics of bacterial populations [6], there is growing interest in the study of proliferating motile matter [7,8]. These are often modeled as interacting particle systems [3,5,9,10], and the number of particles may not be constant in time due to processes such as birth and death. Coupled with individual movement, one can expect new emergent properties. For example, we recently introduced a simple model of *proliferating* motile finite-size particles. Specifically, in [11], we studied both systems of passive disks (where motility has its origins in a thermal bath) and self-propelled disks [12–16] subject to reproduction and death. We analyzed different emerging structural phases [liquid, hexatic, solid, and motility-induced phase separation (MIPS)] [16–22]. These phases result as a consequence of the disks filling the available space, and the phase that is realized depends on parameters such as the birth and death rates, and the motility.

In [11], we focused on a two-dimensional collection of disks (we will also refer to these as particles), which were all taken to be identical; in particular, they have the same size. This is not realistic in many biological applications. In the current work, we analyze the influence on some properties of the system when relaxing this condition and consider a binary mixture of disks of two different sizes [23,24]. In the standard equilibrium system of hard disks (without birth-death events or activity), the two-sizes binary mixture is known to have important effects leading, for example, to the disappearance of the hexatic phase even for very low concentration of small disks [25]. Thus we expect new behavior in a nonequilibrium model of a binary mixture with birth and death dynamics.

We start with a similar concentration for both types (or species) of disks, initially randomly distributed in a two-dimensional space. As the system evolves, particles move, die, and reproduce, eventually filling up space. Due to the death processes, it is possible for one species to go extinct. In reproduction events, a new particle is created in the system, with the same size as the parent, and placed close to it if there is enough room.

As in many real-world systems, reproduction in our model is limited by the available space [26–28]. Under identical conditions, the smaller disks have a higher *a priori* chance to reproduce, and therefore to persist in the long run. Even though the availability of space puts the larger particles at a disadvantage [29,30], we find that depending on motility and demography, the coexistence of both species can occur. In some other cases, we find that the larger particles can dominate the system, i.e., their number is much larger than that of the smaller particles, typically more than 90% of the total particle number.

The main questions that we address are what type of disk dominates the system in the long run, under what conditions both types coexist, and, in the important case of activity-induced phase separation, what the resulting spatial structure is. We are interested in the influence of the birth and death rates and the motilities of the particles on the outcome. In particular, we ask which population survives when the two species compete (due to reproduction limited by size) with different diffusivities [31,32], and we show results that support the prevalence of the fast diffusing type of particle. Our overall aim is to characterize the system behavior for different choices of the model parameters.

In the case of active motion [33–35], we also study what the conditions are under which the spatial distribution of the particles presents coexisting dilute and dense phases, i.e., the MIPS regime. This is, for example, motivated by studies hypothesizing that phase heterogeneity due to MIPS can trigger a transition from swarming behaviour to biofilm formation in some types of bacteria [36]. We analyze the role of

*Contact author: almodovar@ifisc.uib-csic.es
†Contact author: tobias.galla@ifisc.uib-csic.es
‡Contact author: clopez@ifisc.uib-csic.es

this heterogeneity for the dominance dynamics of the binary mixture.

Throughout our analysis, we will mostly concentrate on systems in which the diameter of one type of disk is 20% larger than the other, but we will also discuss other size ratios [37–40].

The remainder of the paper is organized as follows. In Sec. II, we present the model of mobile disks undergoing birth and death dynamics. The main outcomes are presented in Sec. III. A summary and discussion of the findings are contained in Sec. IV.

II. MODEL AND NUMERICAL ALGORITHM

The model is similar to that in [11], but with particles of two different sizes. We consider a two-dimensional system of $N(t) = N_L(t) + N_S(t)$ interacting disks with diameters σ_S and σ_L such that $\sigma_S < \sigma_L$ (S and L stands for "small" and "large," respectively). The particle numbers can change in time, due to birth and death events, as explained below. We consider the overdamped limit and take the friction coefficient to be equal to unity for both species. The motion of disks is then as follows:

$$\dot{\mathbf{r}}_i = \mathbf{F}_i + \mathbf{F}_i^{\rm act} + \sqrt{2D_i}\boldsymbol{\zeta}_i(t), \quad i = 1, \ldots, N(t). \tag{1}$$

If disk i is of the small type, then $D_i = D_S$, and if it is of the large type, then $D_i = D_L$. The variables $\{\boldsymbol{\zeta}_i\}$ are independent Gaussian noise vectors satisfying $\langle \boldsymbol{\zeta}_i \rangle = 0$, $\langle \zeta_{i,a}(t)\zeta_{j,b}(t')\rangle = \delta_{ij}\delta_{ab}\delta(t-t')$ (a and b are the entries of the two-component vectors $\boldsymbol{\zeta}_i$ and $\boldsymbol{\zeta}_j$). No Einstein relation is assumed, and D_L and D_S are taken as parameters of the model. The finite size of the disks is simulated using a truncated Lennard-Jones potential so that the force on particle i resulting from the interaction with the rest of the particles is $\mathbf{F}_i = -\nabla_i \sum_{i\neq j} U(|\mathbf{r}_i - \mathbf{r}_j|)$, where the potential is given by (with $r = |\mathbf{r}_i - \mathbf{r}_j|$)

$$U(r) = 4\varepsilon\left[\left(\frac{\sigma_{ij}}{r}\right)^{12} - \left(\frac{\sigma_{ij}}{r}\right)^{6}\right] + \varepsilon, \tag{2}$$

if $r < 2^{1/6}\sigma_{ij}$, and $U(r) = 0$ if $r > 2^{1/6}\sigma_{ij}$. The quantity $\sigma_{ij} > 0$ is defined from the Lorentz-Berthelot rule as $\sigma_{ij} = (\sigma_i + \sigma_j)/2$, where σ_i and σ_j are the diameters of disks i and j, respectively. Thus, σ_{ij} reflects the effective distance between the two disks. The parameter ε is an energy scale [41,42].

In some of our numerical experiments, particles are self-propelled. We model this using active forces

$$\mathbf{F}_i^{\rm act} = v_i \mathbf{n}[\theta_i(t)] \tag{3}$$

of constant modulus $v_i = \{v_L, v_s\}$ (typically called activity or velocity) and with a direction given by the unit vector $\mathbf{n}(\theta_i) = (\cos\theta_i, \sin\theta_i)$. The angle θ_i for disk i performs diffusive motion, $\dot{\theta}_i(t) = \sqrt{2D_r}\eta_i(t)$. The term η_i represents a zero-mean Gaussian noise with $\langle \eta_i(t)\eta_j(t')\rangle = \delta_{ij}\delta(t-t')$.

In addition to movement and interaction, disks may randomly self-replicate or die, so that the number of disks of each type, $N_L(t)$ and $N_S(t)$, can change with time. These events occur as follows (see [11] for further details of the algorithm):

(i) Death occurs as a Poisson process. Each existing particle dies with per capita rate δ. Particles that die are removed from the system.

(ii) Potential births are triggered with per capita rate β_L for large disks, and β_S for small disks. The diameter of the potential offspring is identical to that of the parent. The birth event only occurs if there is sufficient space around the parent particle to place the offspring without overlapping with any other disk. If there is no space, no birth event occurs. This means that not all potential reproduction events complete.

We always assume that the growth rates β_S and β_L are larger than the death rate (the latter is taken to be equal for all the disks), i.e., $\beta_L, \beta_S > \delta$. At long times, the system reaches a stationary state. The numbers of disks of each type in this state is such that the mean effective birth rate for each species is equal to the death rate.

In the next sections, we study this steady state while varying one or two model parameters at a time (e.g., the diffusivity of both types of particles, the growth rates, or activity). Our main objective is to study what type of disk dominates and under what conditions there is coexistence.

III. RESULTS

We consider a two-dimensional box of length $L_s = 150$ with periodic boundary conditions, $\delta = 0.01$, and, for the most part, $\sigma_S = 1.0$ and $\sigma_L = 1.2$, supplemented by some discussion of other choices of the diameters. For simplicity, we set $\varepsilon = 1.0$ and $D_r = 1.0$. Simulation results are independent of δ, whose role is mostly to set the timescale needed to reach the steady state [11]. We start with 250 particles of each size, together occupying around 8% of the total area. We compute the packing fraction for particles of each type. We write these as $\phi_\alpha(t) = N_\alpha(t)\pi(\sigma_\alpha/2)^2/L_s^2$ for $\alpha \in \{L, S\}$, where $N_\alpha(t)$ is the number of particles of type α at time t.

We study passive particles in Sec. III A. Systems of active particles are discussed in Sec. III B.

A. Passive particles

We set $\mathbf{F}_i^{\rm act} = 0$ and study the effects of the parameters of the demographic dynamics, and of the diffusivities separately.

1. Effects of the birth and death rates

We fix the diffusivities to low values (i.e., the timescale of a disk to move a distance of the order of several diameters is large compared to its typical lifetime), $D_L = D_S = 0.001$, to focus on the effects of the birth and death dynamics. Since reproduction is limited by the available space, we naively expect only the smaller disks to be present in the long run when the raw birth rates of both types are similar. However, the outcome may be different if the birth rate for the larger particles is much larger than that of the smaller type. This is indeed what we observe in the numerical experiments shown in Fig. 1.

In the upper row of Fig. 1, we plot snapshots of the spatial distribution of disks in the stationary state. Smaller particles are shown in red, larger ones in green. The growth rate of the small particles is lower than that of the larger particles in Figs. 1(a)–1(c), but the ratio β_L/β_S increases from left to right. In Fig. 1(a), we observe the extinction of the larger particles; in Fig. 1(b), we find balanced coexistence throughout the simulation; and in Fig. 1(c), the ratio β_L/β_S is sufficiently large

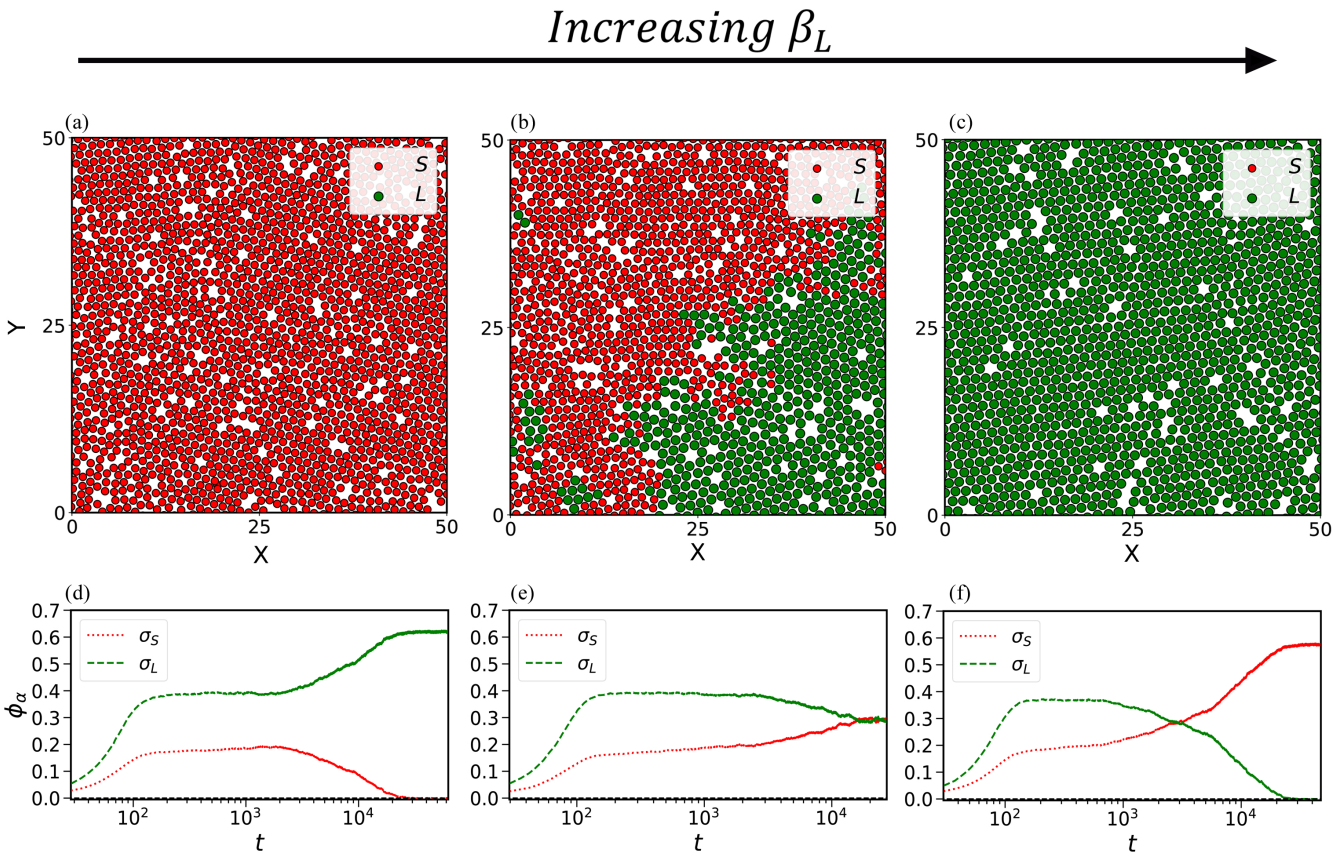

FIG. 1. (a)–(c) Snapshots of the spatial distribution of passive disks in space at long times (only a part of the full size $L_s = 150$ is shown). (d)–(f) The temporal evolution of the packing fraction starting with a random configuration of 250 disks of each type. The snapshots in (a)–(c) are taken at the end of the time series in (d)–(f), respectively. In each column, we have used different values of β_L, at fixed $\beta_S = 0.05$, and $\beta_L = 0.06, 0.062, 0.065$ from left to right. The remaining parameters are $\delta = 0.01$, $D = 0.001$, $\sigma_L/\sigma_S = 1.2$.

for the larger disks to fully dominate (the smaller particles go extinct). In the lower row of Fig. 1, we plot the corresponding time evolution of the packing fractions (the snapshots in the upper row are taken at the final time of the lower ones). These time series confirm the extinction of the larger type of particle [Fig. 1(d)], coexistence [Fig. 1(e)], and the extinction of the smaller type [Fig. 1(f)]. In all three situations, and regardless of the final fate of the larger particles, there is initially a faster increase of the packing of the larger particles. This is because $\beta_L > \beta_S$ in all panels in Fig. 1.

In Fig. 2(a), we plot the phase diagram in the plane of birth rates for the two species (each divided by the death rate $\delta = 0.01$). The colored heat map indicates the normalized packing fraction $\phi_S/(\phi_S + \phi_L)$ of the smaller disks. In Fig. 2(b), we show the respective packing fractions of both types when varying β_L, for fixed β_S. This corresponds to a vertical cut of the phase diagram in Fig. 2(a). The dominance of the smaller type at low β_L, coexistence at intermediate values, and dominance of the larger disks at high β_L are clearly visible.

The coexistence of both species occurs in a very limited region of the diagram, i.e., around a small area near a specific line in the (β_S, β_L) plane. An approximate characterization of this coexistence curve can be obtained from a simple description of the dynamics in terms of rate equations. To construct these equations with proper parameters, we first consider only one type of disk in isolation, neglect fluctuations and any notion of space. We use a Lotka-Volterra model to describe the combination of death events and growth limited by volume exclusion [43],

$$\frac{dN}{dt} = -\delta N + \hat{\beta} N\left(1 - \frac{N}{N_{\max}}\right), \tag{4}$$

where the term in the brackets ensures that the growth dynamics stops as N reaches $N_{\max}$; δ is the death rate and $\hat{\beta}$ is an effective growth rate.

This effective growth rate is a fitting parameter introduced in this very simple description to take into account that the actual birth rate is limited by the available space, and therefore not equal to the raw birth rate β. We take $\hat{\beta} = a\beta$, where a is an unknown adimensional coefficient. In [11], we observed that the steady number of disks in a single-species model depends in a nontrivial way on the birth and death rates, the size of the particles, and on the diffusion coefficient. Thus, in this description, we use $a > 0$ and $N_{\max}$ as fitting parameters.

We rewrite Eq. (4) in the standard form,

$$dN/dt = rN(1 - N/K), \tag{5}$$

with $r = a\beta - \delta$. The carrying capacity $K = N_{\max}(1 - \frac{\delta}{a\beta})$ is the effective long-time number of disks in the system.

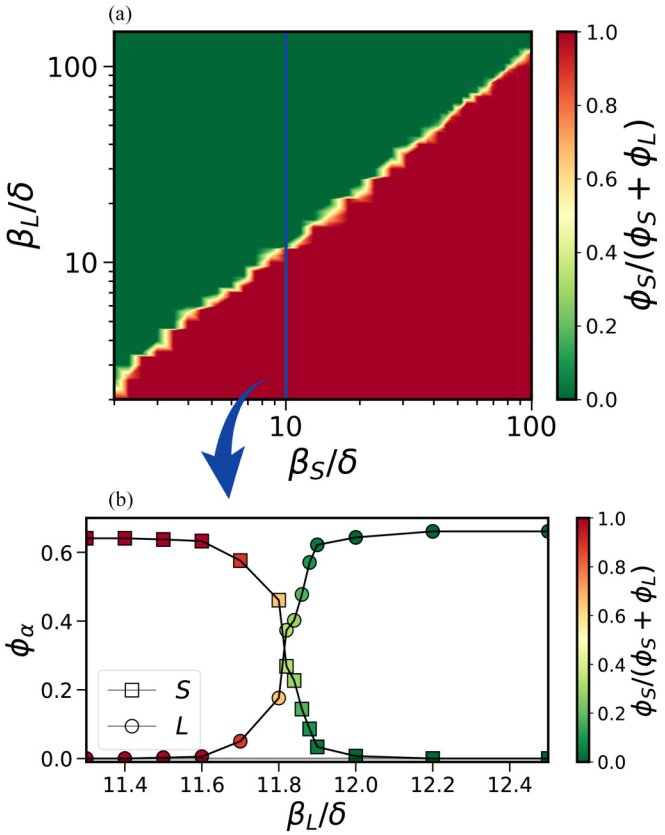

FIG. 2. Coexistence diagram for the system of passive particles in the plane spanned by the birth rates β_S and β_L. (a) Color indicates where in parameter space either type of particle dominates or if there is coexistence. (b) Vertical cut in the phase diagram in (a) for $\beta_S/\delta = 10$ (as indicated by the blue line) showing the packing fractions for both types of disks. The colors of the symbols represent the fraction of small particles in the system. $\delta = 0.01$, $\sigma_S = 1.0$, and $\sigma_L = 1.2$. The simulation data represented in the phase diagram are derived from time-averaged values in the long time for a single realization.

To verify the validity of the logistic-growth approach, we have carried out simulations of the model in which all particles have the same size, using a small diffusion coefficient, $D = 0.001$. In the long time, we compute the packing fraction $\phi_\infty = N(t\to\infty)\pi(\sigma/2)^2/L_s^2$. We do this for several different disk sizes ($\sigma = 1.0, 1.2, 1.4$) and for some values of β to check the relationship $\phi_{\rm stat} = K\pi(\sigma/2)^2/L_s^2 = N_{\rm max}\pi(\sigma/2)^2/L_s^2(1-\frac{\delta}{a\beta})$ (the stationary packing fraction of the Lotka-Volterra equation). The results are shown in Fig. 3. There is a good collapse of all the plots for the different values of σ, and the best fit to the expression of ϕ_∞ is obtained for $\phi_{\rm max} = N_{\rm max}\pi(\sigma/2)^2/L_s^2 = 0.7$, $a = 1.5$. This confirms that the logistic description with suitable effective parameters can be used to describe the stationary state with a single type of particle.

The Lotka-Volterra model can be generalized to the case of a binary mixture of disks. This approximate description can be useful to study the influence of one type of disks on the other, in particular, attending to their different sizes and growth rates. We assume the following Lotka-Volterra competition dynamics between the two species (which we again label S and L for "small" and "large" disks, respectively) [44]:

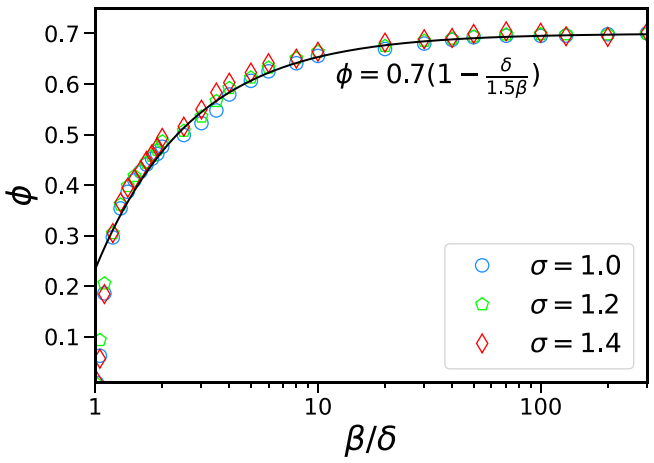

FIG. 3. Long-time average packing fraction ϕ_∞ for a system of only one type of disks as a function of the rate β and $\delta = 0.01$. The plots correspond to different disk sizes σ as the symbols indicate. The black line corresponds to the best fitted curve for $a = 1.5$, and $\phi_{\rm max} = 0.7$.

$$\frac{dN_L}{dt} = -\delta N_L + a\beta_L\left(1-\frac{N_L+\alpha_L N_S}{N_{L,\rm max}}\right)N_L,$$
$$\frac{dN_S}{dt} = -\delta N_S + a\beta_S\left(1-\frac{N_S+\alpha_S N_L}{N_{S,\rm max}}\right)N_S. \quad (6)$$

The term $\alpha_L N_S$ ($\alpha_S N_L$) is the decline of the growth rate of N_L (N_S) due to the presence of the smaller (larger) disks. The quantities $N_{S,\rm max}$ and $N_{L,\rm max}$ are the number of particles for either species at which no further growth can occur.

The dependence of the interaction terms on the ratio of disk sizes becomes more apparent if we write this equation in terms of packing fractions,

$$\frac{d\phi_L}{dt} = -\delta\phi_L + a\beta_L\left(1-\frac{\phi_L+\alpha_L\frac{\sigma_L^2}{\sigma_S^2}\phi_S}{\phi_{L,\rm max}}\right)\phi_L,$$
$$\frac{d\phi_S}{dt} = -\delta\phi_S + a\beta_S\left(1-\frac{\phi_S+\alpha_S\frac{\sigma_S^2}{\sigma_L^2}\phi_L}{\phi_{S,\rm max}}\right)\phi_S. \quad (7)$$

Now, $\phi_{\alpha,\rm max} = N_{\alpha,\rm max}\pi(\sigma_\alpha/2)^2/L_s^2$ ($\alpha = L, S$). We assume that α_L and α_S depend on the demographic parameters of the system (β_L, β_S), and as detailed in the Appendix A. Fitting to simulation data, we find

$$\alpha_L \approx \left(\frac{\beta_S}{\beta_L}\right)^{1/4},$$
$$\alpha_S \approx \left(\frac{\beta_L}{\beta_S}\right)^{1/4}. \quad (8)$$

These relations characterize the tradeoff between geometry and demography (reproduction) in the competition dynamics. For example, the coefficient in the growth rate for the larger disks, $\alpha_L\frac{\sigma_L^2}{\sigma_S^2} = \frac{\sigma_L^2}{\sigma_S^2}(\frac{\beta_S}{\beta_L})^{1/4}$, increases proportionally to $(\sigma_L/\sigma_S)^2$, while its dependence on the relative birth rates is much weaker and only scales as $(\beta_S/\beta_L)^{1/4}$.

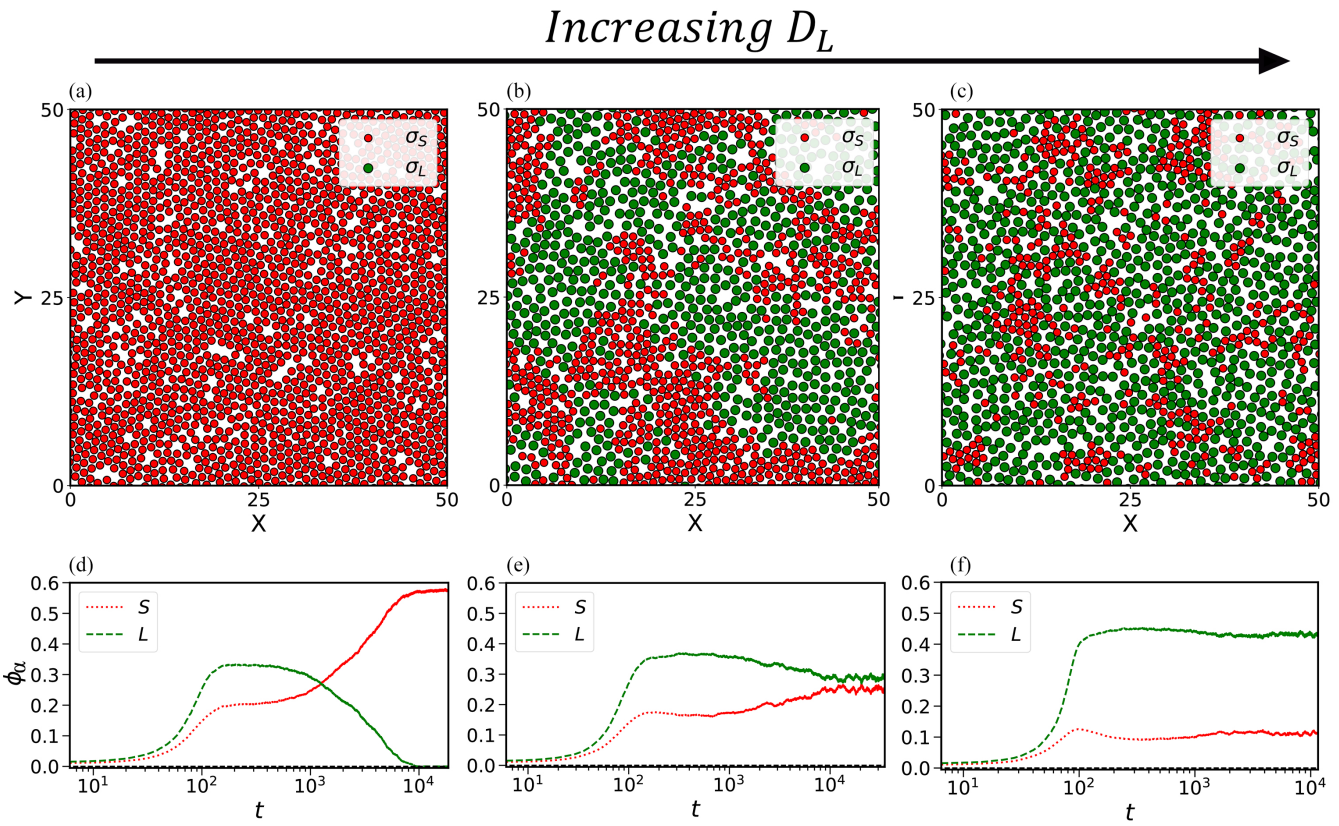

FIG. 4. (a)–(c) Snapshots of the spatial distribution of passive disks space at long times (graphs only show a part of the full system, which has lateral size $L_s = 150$). (d)–(f) The corresponding time evolution of the packing fractions for both species, starting with a random configuration of 250 disks of each type. In the different columns, we have used different values of D_L and $D_S = 0.001$: $D_L = 0.01$, 0.02, 1.0 from left to right. Remaining parameters are $\delta = 0.01$, $\beta = 0.05$, $\sigma_L/\sigma_S = 1.2$.

2. *The role of diffusion*

In this section, we study the case in which both types of passive disks have the same birth and death rates, but where their diffusion coefficients are different. In biological applications, situations of this type have given rise to contradictory results (albeit under very different settings) so that diffusing faster provides a competitive advantage [31] or can be detrimental [32]). Thus, one of the main questions that we address is if high or low diffusivity can provide a selective advantage for either of the two competing populations.

In the upper row of Fig. 4, we show the spatial distribution of disks at long times, for different D_L and leaving all other model parameters fixed. In Fig. 4(a) (small ratio D_L/D_S), the smaller particles dominate the system. In Fig. 4(b) (intermediate D_L/D_S), there is a balance of both types of disks, and when D_L/D_S is sufficiently high [Fig. 4(c)], the larger disks occupy most of the space. Figures 4(d)–4(f) show the time evolution of the packing fractions of both types in simulations starting with 250 particles of each size. The corresponding phase diagram, for $\sigma_L/\sigma_S = 1.2$, is shown in Fig. 5(a). Increasing the diffusivity of either species promotes an increased relative abundance of that species. This is because larger diffusivity for a given particle means it effectively occupies more space where others cannot place their offspring. In particular, we observe a transition between phases in which the system is predominantly filled by the smaller particles to one in which it is mostly filled by larger particles.

We conclude that increasing diffusivity of the larger disks can reverse the competitive advantage of the smaller ones. We have seen that due to the space-limited birth dynamics, diffusion is "related" to particle size. However, the details of this relationship are subtle. We observe that diffusion increases the survival probability of a particle type. This is against the intuition that the effective particle size would increase with diffusivity, and that this would thus lead to a reduction of the particles' effective birth rate. One possible mechanism leading to this is that larger diffusivity might increase the effective size of a given particle as far as the interaction with other particles is concerned. Suppose the diffusivity of a focal particle is increased. The particle will "disturb" other particles in its surroundings, thus leading to a reduction of these particles' birth rate. This then makes space for the focal particle itself to reproduce. At difference with the results of the previous section (Fig. 1), the dominance of larger disks for high D_L/D_S is not complete though. Instead, we find a remaining population of smaller disks occupying about 10–15% of space until the end of our simulations (i.e., $\phi_S = 0.1$–0.15); see Fig. 5(b). We attribute this to interstitial holes, i.e., empty space between the disks, noting that the effect is more pronounced [i.e., $\phi_S/(\phi_S + \phi_L)$ becomes larger] when the ratio σ_L/σ_S is increased (see Fig. 6).

An exception to the survival of the smaller disks can be observed in a region in (D_S, D_L) space in which the larger disks almost completely dominate the system [dark green

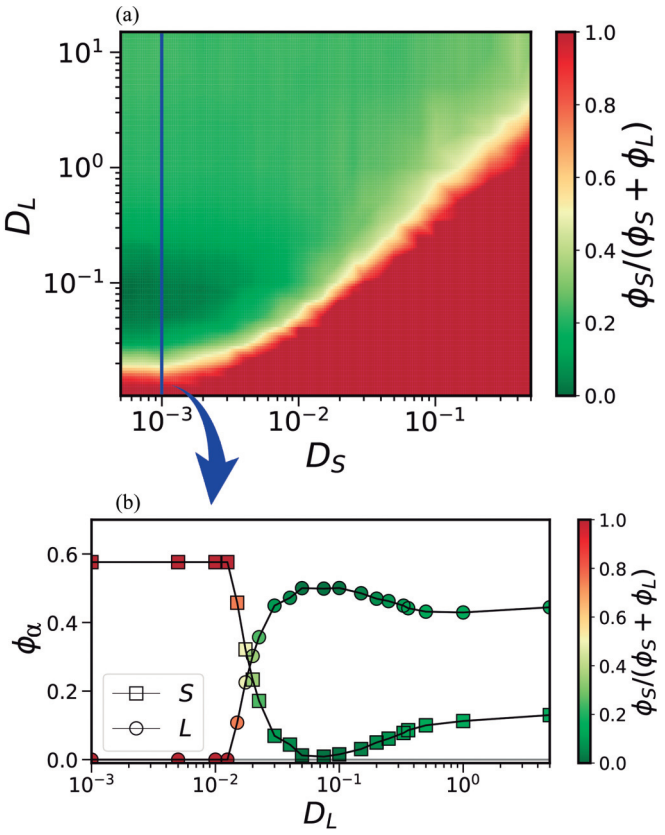

FIG. 5. Phase diagram in the space of diffusivities, D_S and D_L. (a) Background color indicates the relative filling fraction of the two type of disks. In the red region, the smaller particles fill most of the space; in the green region, the larger particles dominate. (b) Long-time average packing fractions for both species as a function of D_L, for fixed $D_S = 0.001$. The colors of the symbols indicate the relative amount of space occupied by the small particles. Model parameters are $\delta = 0.01$, $\beta_L = \beta_S = 0.05$, $\sigma_S = 1.0$, $\sigma_L = 1.2$.

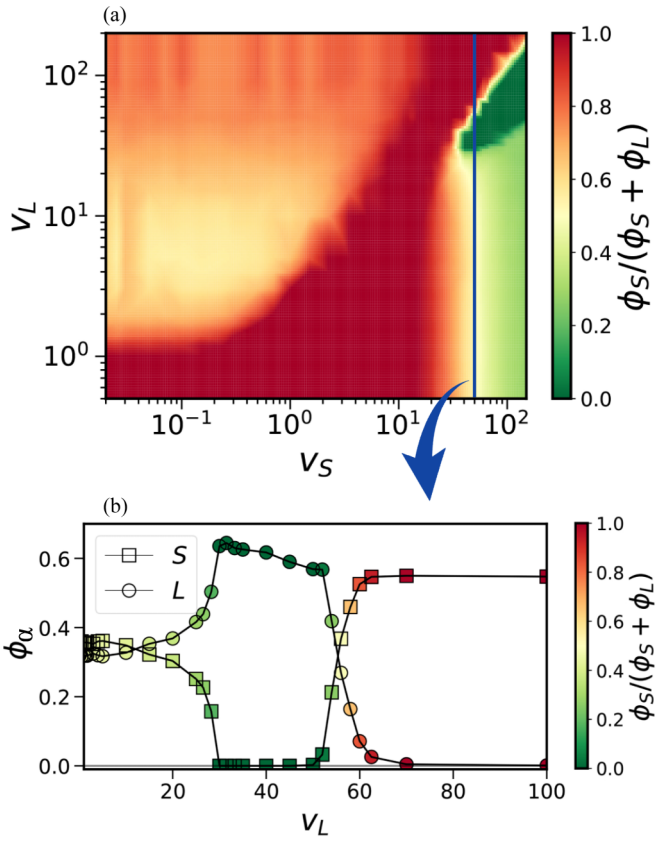

FIG. 7. (a) Phase diagram of the system with active disks in the (v_L, v_S) plane. Background color represents the normalized packing fraction of the smaller particles (darker-red color indicates dominance of the smaller type; darker-green color indicates dominance of the larger type). (b) Long-time average packing fractions for both species as a function of v_L for fixed $v_S = 50$. The colors of the symbols indicate the relative space occupied by the small particles. Model parameters are $\delta = 0.01$, $\beta_L = \beta_S = 0.05$, $\sigma_S = 1.0$, $\sigma_L = 1.2$.

to the lower left in Fig. 5(a)]. This dominance only occurs when D_S is small enough so that the movement of the smaller disks is negligible with respect to their lifetime. This region disappears as the ratio σ_L/σ_S becomes larger (see Fig. 6), so that we think it is because small disks may occupy the interstitial holes.

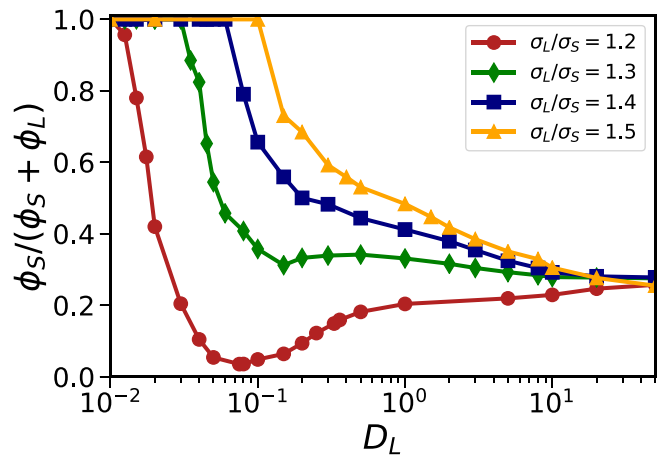

FIG. 6. Normalized packing fraction of small particles vs D_L for different values of σ_L/σ_S as indicated. Same remaining parameters as in Fig. 5.

B. Active particles

We consider systems in which both types of disks are self-propelled, possibly with different values of the propulsion velocities v_L and v_S. The remaining parameters are set to the same: $\beta_L = \beta_S = \beta$, $D_L = D_S = D$, and $\delta = 0.01$.

We first take a birth rate of $\beta = 0.05$ and diffusivity of $D = 0.05$. Under these conditions, without activity, the system is in a liquid state, which means that the packing fraction of both types is low and there is no ordering. Also the system reaches the steady state faster. Our motivation for this choice is that we aim at analyzing MIPS, which is typically not observed for large values of the packing fraction (solid phase) [11,15].

In the previous section, we have shown that Brownian mobility provides an advantage in the competition for space between the two types of disks. Given that self-propulsion yields comparable effects (at low velocities) to diffusivity [45,46], we expect, in this low activity regime, similar

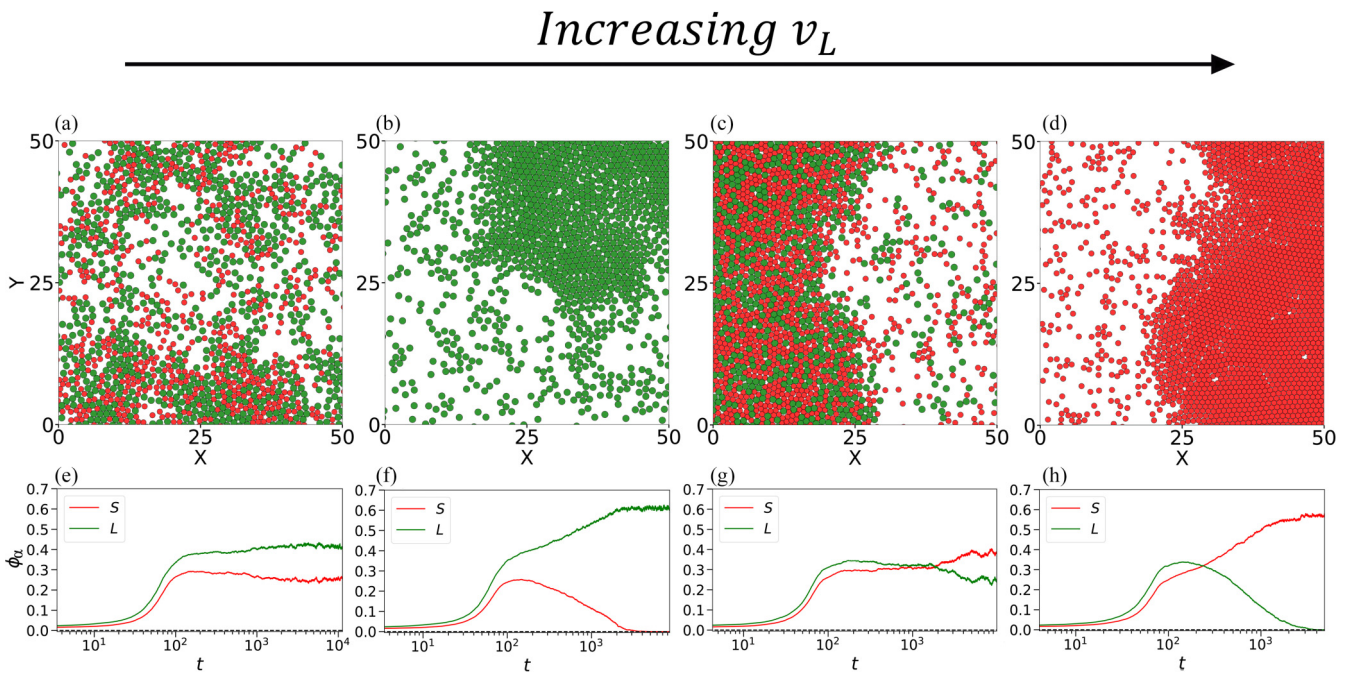

FIG. 8. (a)–(d) Snapshots of the spatial distribution of active disks space at long times (only a part of the full size $L_s = 150$). (e)–(h) The temporal evolution of the packing fraction starting with a random configuration of $250 + 250$ disks. In addition, for each column, we have used different values of v_L and $v_S = 50$. The values used are $v_L = 25$, 40, 56, and 70 from left to right.

outcomes for active particles. However, MIPS typically appears when activity is large, and thus we study this regime in detail by varying the self-propulsion coefficients of both types of disks, and compute the average packing fraction of each species at long times.

The resulting phase diagram, obtained for $\sigma_L/\sigma_S = 1.2$, is shown in Fig. 7(a). When the activity of both types of disks is sufficiently low, the smaller disks dominate the system. As v_L increases (keeping v_S fixed at a sufficiently small value), a transition to coexistence is found. This coexistence remains as the activity of the larger particles is further increased. We find interesting behavior for sufficiently large v_S. This is the region of MIPS. We observe that coexistence can be reached for low and intermediate values of v_L [see Fig. 7(b)]. In between, there is a range of values where large particles dominate, and for very high v_L small particles dominate the system.

Which type of particle survives (or the presence of coexistence) results from a complicated interplay between the separation in dense and diluted phases formed of both species in nonsteady conditions because of activity, and the birth-death dynamics which is itself mediated by the spatial distribution of disks. This is shown in the upper row of Fig. 8 with some examples of the disk distribution at long times for $v_S = 50$ and different values of v_L. In Fig. 8(a), there is coexistence for sufficiently small v_L. As we increase v_L, the smaller species becomes extinct (dark-green region in the phase diagram) Fig. 8(b). As v_L is increased further, coexistence is observed again and both species show MIPS [see Fig. 8(c)]. For even higher values of v_L, the large disks become extinct [see Fig. 8(d)]. In the lower row, we show the corresponding time evolutions of the packing fractions of both types of particles, starting from a configuration with 250 particles of each.

Let us next characterize the emerging spatial structures when there is coexistence. To do this, we compute the distribution of local packing fractions of large disks, $P(\phi_L)$, and small ones, $P(\phi_S)$. These are obtained from the local packing fraction of either species at each location in space. MIPS is characterized by a double-peaked distribution, with the two peaks corresponding to the dense and diluted phases, respectively [15]. In Fig. 9(a), we plot $P(\phi_S)$ and $P(\phi_L)$ corresponding to two situations: (i) small particles with very low $v_S = 0.1$ and large particles with low $v_L = 10$ (the two distributions are plotted in red); and (ii) small particles again with $v_S = 0.1$, but large particles with high $v_L = 150$. These scenarios correspond, respectively, to the cases where (if the two types were in isolation without the presence of the other) (a) neither small nor large disks would form MIPS, and (b) small disks would not form MIPS, but large ones would because they have a high v_L. However, when both types of particles are present in the system, the distribution of local packing fractions is single peaked, and there is no separation between dilute and dense phases.

Instead, in Fig. 9(b), we use a higher value of $v_S = 50$ and two different values of v_L: $v_L = 25$ for which there would be no MIPS for the large particles in isolation, and $v_L = 56$ for which there would be MIPS. Now, $P(\phi_L)$ and $P(\phi_S)$ are double peaked, that is, both types of disks have a dense and a dilute phase. These results indicate that the two species arrange in the same spatial distribution when they coexist. Either both display a single phase or both species show MIPS.

Finally, in Fig. 10, we plot the normalized packing fraction for the smaller types of disks when v_L varies (keeping $v_S = 50$ fixed, i.e., within the MIPS region) and for several values of the ratio of size particles. When we increase σ_L/σ_S, the effect

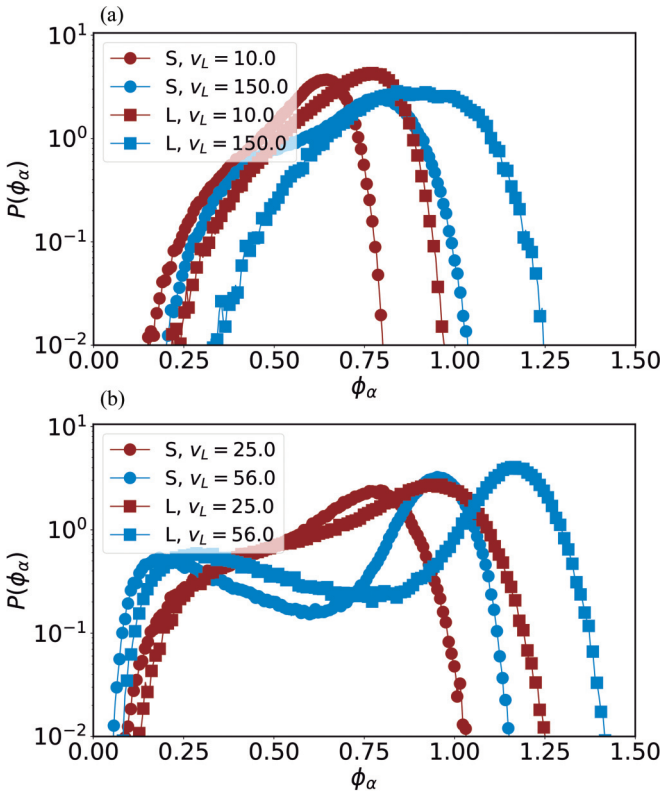

FIG. 9. Distribution of the local packing fraction for different values of activity in configurations where both disks types coexist. (a) $v_S = 0.1$. (b) $v_S = 50$. The v_L value is shown in the legend.

of the interstices becomes more pronounced, which causes the small particles' packing fraction to increase. For the same reason, the region in Fig. 10 in which the smaller particles go extinct reduces. In other words, as σ_L/σ_S increases, the large particles need a higher value of activity to form MIPS. This results in a higher value of v_L for the small particles to go extinct.

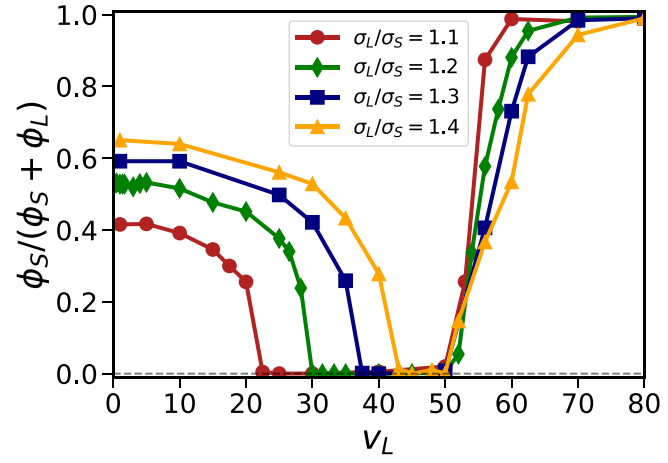

FIG. 10. Normalized packing fraction of the smaller type of particle vs v_L for different values of σ_L/σ_S as indicated in the legends. $v_S = 50$, and same remaining parameters as in Fig. 7.

IV. SUMMARY AND DISCUSSIONS

The interplay between motility and proliferation is fundamental for many biological processes. In this work, we have studied a binary mixture of two types of motile disks with different sizes and undergoing birth and death dynamics. At difference with our previous work [11] where we concentrated on the spatial structure formed by a single population of identical disks, in this work we have studied the conditions for coexistence and which of the two types does not go extinct in the long time. Since the birth probability is limited by size, smaller disks have larger chances to reproduce (when the remaining characteristics are identical). Thus we focused on the conditions under which this is reversed, i.e., larger disks survive or there is coexistence of both types of disks. We have considered two main cases: passive and self-propelled disks. For passive particles, we have discussed the role of growth rates and diffusivities, and have obtained typical phase diagrams when the ratio of the particles' sizes is $\sigma_L/\sigma_s = 1.2$, but also discussed it for other ratios, unveiling the role of interstices. We observe that Brownian mobility provides an advantage such that the larger particles, with less chances to reproduce, can coexist with the smaller or even dominate in the steady state when they diffuse faster.

We have analyzed the role of activity and have shown that as expected, it is similar to that of diffusivity when self-propelled velocities have low values. However, when MIPS is present (typically obtained for larger values of activities), the coexistence dynamics changes and the typical situation is a coexistence of both species, with both showing the same diluted and dense phases.

From our study, we learn that while size may initially appear as a limiting proliferation factor, the interplay with other processes can mitigate its effects. More specifically, our main findings are as follows: (i) the interaction coefficients of the two species can be interpreted as a ratio of the two birth rates, (ii) a larger diffusion coefficient can provide a competitive advantage, (iii) activity can induce coexistence, and (iv) activity can induce that the particles that initially had less chance of survival completely dominate the system. Further work should be devoted to analyze the spatial structure in the different situations that we have described and, in particular, the influence on the hexatic and solid phases, if any, of the binary mixture with demography. Extensions of the model could allow for partial overlap of the offspring with the parent. This would likely lead to a larger packing fraction. Therefore, we speculate that allowing partial overlap would produce similar effects as increasing the birth rate.

Concerning biological applications, the main motivation for our work, where populations are characterized by large diversity, it is of great interest to consider not only two disks sizes, but a whole size distribution, and also of the other parameters such as the growth rates and the self-propulsion velocities.

ACKNOWLEDGMENTS

A.A and C.L. acknowledge Grant No. LAMARCA PID2021-123352OB-C32 funded by MCIN/AEI/10.13039/501100011033323 and FEDER "Una manera de hacer

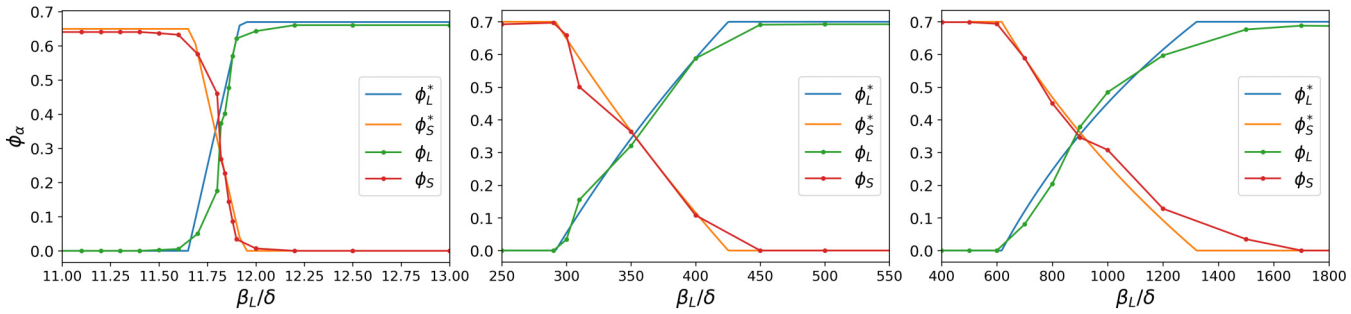

FIG. 11. Long-time average packing fractions for both species as a function of β_L/δ, for fixed $\beta_S = 0.1$ (left) and $\beta_S = 0.85$ (middle and right), and $\delta = 0.01$. ϕ_α^* obtained from Eq. (A4) and ϕ_α from particle simulations. From left to right: $\sigma_L/\sigma_S = 1.2, 1.3, 1.4$.

Europa". T.G. acknowledges partial financial support from the Agencia Estatal de Investigación and Fondo Europeo de Desarrollo Regional (FEDER, UE) under Project No. APASOS (PID2021-122256NB-C21, PID2021-122256NB-C22), and the Maria de Maeztu programme for Units of Excellence, Grant No. CEX2021-001164-M funded by MCIN/AEI/10.13039/501100011033.

APPENDIX

The parameters for which both species coexist can be approximated from the nonzero fixed points of Eq. (7),

$$\phi_S^* = \kappa_S - \alpha_S \phi_L^* \left(\frac{\sigma_S}{\sigma_L}\right)^2,$$
$$\phi_S^* = \frac{1}{\alpha_L}(\kappa_L - \phi_L^*)\left(\frac{\sigma_S}{\sigma_L}\right)^2, \tag{A1}$$

with

$$\kappa_S = \frac{a\beta_S - \delta}{a\beta_S}\phi_{S,\max},$$
$$\kappa_L = \frac{a\beta_L - \delta}{a\beta_L}\phi_{L,\max}. \tag{A2}$$

Both equalities are fulfilled at the same time in the coexistence region. Furthermore, recall that $\phi_{S,\max} = \phi_{L,\max}$, since the maximum value does not depend on either the type of particle or the size of the system. Now, we make the ansatz

$$\alpha_S = c_S(\beta_L/\beta_S)^\gamma,$$
$$\alpha_L = c_L(\beta_S/\beta_L)^\gamma, \tag{A3}$$

where c_S, c_L, and γ are constants.

We have assumed symmetry in the interaction of the species, so that both species have the same exponent γ. Inserting the ansatz (A3) in Eq. (A1), we obtain an expression for the packing fraction with explicit dependence on the demographic rates,

$$\phi_S^* = \frac{1}{1 - c_L c_S}\left[\kappa_S - \kappa_L c_S \left(\frac{\beta_L}{\beta_S}\right)^\gamma \left(\frac{\sigma_S}{\sigma_L}\right)^2\right],$$
$$\phi_L^* = \frac{1}{1 - c_L c_S}\left[\kappa_L - \kappa_S c_L \left(\frac{\beta_S}{\beta_L}\right)^\gamma \left(\frac{\sigma_L}{\sigma_S}\right)^2\right]. \tag{A4}$$

These expressions predict the value of the steady packing fractions at each point of the diagram (β_L, β_S) inside the coexistence region. In the region where only large (small) particles are found, we have $\phi_L^* = \kappa_L$ and $\phi_S^* = 0$ ($\phi_L^* = 0$ and $\phi_S^* = \kappa_S$).

We have carried out a series of numerical experiments for various values of δ, σ_L, σ_S (not shown) beyond those used in Fig. 2 and have observed that the phase diagram is almost independent of the value of δ (always assuming $\beta > \delta$), and the ratio σ_L/σ_S. The coefficients c_L, c_S, and γ in Eq. (A4) can be obtained from fits of the packing fraction (see Fig. 11). We compute the difference between the packing fraction obtained from Eq. (A4) and the one obtained from the numerical simulations of the particle model for different values of δ, σ_S, σ_L, β_S, β_L. Then, we minimize the sum of all the differences.

From these simulations, the best fit is obtained for $c_L = 0.69$, $c_S = 1.34$, and $\gamma = 1/8$.

[1] R. Alert and X. Trepat, Annu. Rev. Condens. Matter Phys. **11**, 77 (2020).
[2] R. Alert and X. Trepat, Phys. Today **74**(6), 30 (2021).
[3] N. Sepúlveda, L. Petitjean, O. Cochet, E. Grasland-Mongrain, P. Silberzan, and V. Hakim, PLoS Comput. Biol. **9**, e1002944 (2013).
[4] T. E. Angelini, E. Hannezo, X. Trepat, M. Marquez, J. J. Fredberg, and D. A. Weitz, Proc. Natl. Acad. Sci. USA **108**, 4714 (2011).
[5] C. A. M. La Porta and S. Zapperi, *The Physics of Cancer* (Cambridge University Press, Cambridge, England, 2017).
[6] B. Szabó, G. J. Szöllösi, B. Gönci, Z. Jurányi, D. Selmeczi, and T. Vicsek, Phys. Rev. E **74**, 061908 (2006).
[7] O. Hallatschek, S. S. Datta, K. Drescher, J. Dunkel, J. Elgeti, B. Waclaw, and N. S. Wingreen, Nat. Rev. Phys. **5**, 407 (2023).
[8] Y. Tang, S. Chen, M. Bowick, and D. Bi, arXiv:2303.00129 [Phys. Rev. Lett. (to be published)].
[9] Y. Kim, S. Joo, W. K. Kim, and J.-H. Jeon, Macromol. **55**, 7136 (2022).

[10] Y. Du, H. Jiang, and Z. Hou, Soft Matter **15**, 2020 (2019).
[11] A. Almodóvar, T. Galla, and C. López, Phys. Rev. E **106**, 054130 (2022).
[12] P. Romanczuk, M. Bär, W. Ebeling, B. Lindner, and L. Schimansky-Geier, Eur. Phys. J.: Spec. Top. **202**, 1 (2012).
[13] B. ten Hagen, S. van Teeffelen, and H. Löwen, J. Phys.: Condens. Matter **23**, 194119 (2011).
[14] Y. Fily and M. C. Marchetti, Phys. Rev. Lett. **108**, 235702 (2012).
[15] P. Digregorio, D. Levis, A. Suma, L. F. Cugliandolo, G. Gonnella, and I. Pagonabarraga, Phys. Rev. Lett. **121**, 098003 (2018).
[16] L. Caprini, U. M. B. Marconi, C. Maggi, M. Paoluzzi, and A. Puglisi, Phys. Rev. Res. **2**, 023321 (2020).
[17] E. P. Bernard and W. Krauth, Phys. Rev. Lett. **107**, 155704 (2011).
[18] J. U. Klamser, S. C. Kapfer, and W. Krauth, Nat. Commun. **9**, 5045 (2018).
[19] F. F. Abraham, Phys. Rep. **80**, 340 (1981).
[20] D. R. Nelson and B. I. Halperin, Phys. Rev. B **19**, 2457 (1979).
[21] M. E. Cates and J. Tailleur, Annu. Rev. Condens. Matter Phys. **6**, 219 (2015).
[22] I. Buttinoni, J. Bialké, F. Kümmel, H. Löwen, C. Bechinger, and T. Speck, Phys. Rev. Lett. **110**, 238301 (2013).
[23] T. Biben and J.-P. Hansen, Phys. Rev. Lett. **66**, 2215 (1991).
[24] D. Frenkel and A. A. Louis, Phys. Rev. Lett. **68**, 3363 (1992).
[25] J. Russo and N. B. Wilding, Phys. Rev. Lett. **119**, 115702 (2017).
[26] G. Larwood and B. Rosen, *Biology and Systematics of Colonial Organisms*, Physiological Ecology (Systematics Association, London, 1979).
[27] J. B. C. Jackson, Am. Nat. **111**, 743 (1977).
[28] L. M. Ponczek and N. W. Blackstone, Biol. Bull. **201**, 76 (2001).
[29] S. Das, S. Ghosh, and R. Chelakkot, Phys. Rev. E **102**, 032619 (2020).
[30] A. Reversat, F. Gaertner, J. Merrin, J. Stopp, S. Tasciyan, J. Aguilera, I. de Vries, R. Hauschild, M. Hons, M. Piel, A. Callan-Jones, R. Voituriez, and M. Sixt, Nature (London) **582**, 582 (2020).
[31] S. Pigolotti and R. Benzi, Phys. Rev. Lett. **112**, 188102 (2014).
[32] E. Heinsalu, E. Hernández-García, and C. Lopez, Phys. Rev. E **85**, 041105 (2012).
[33] M. C. Marchetti, J. F. Joanny, S. Ramaswamy, T. B. Liverpool, J. Prost, M. Rao, and R. A. Simha, Rev. Mod. Phys. **85**, 1143 (2013).
[34] C. Bechinger, R. Di Leonardo, H. Löwen, C. Reichhardt, G. Volpe, and G. Volpe, Rev. Mod. Phys. **88**, 045006 (2016).
[35] V. Hakim and P. Silberzan, Rep. Prog. Phys. **80**, 076601 (2017).
[36] I. Grobas, M. Polin, and M. Asally, eLife **10**, e62632 (2021).
[37] P. K. Bommineni, N. R. Varela-Rosales, M. Klement, and M. Engel, Phys. Rev. Lett. **122**, 128005 (2019).
[38] P. Sampedro Ruiz, Q.-l. Lei, and R. Ni, Commun. Phys. **2**, 70 (2019).
[39] P. Sampedro Ruiz and R. Ni, J. Chem. Phys. **153**, 174501 (2020).
[40] S. Kumar, J. P. Singh, D. Giri, and S. Mishra, Phys. Rev. E **104**, 024601 (2021).
[41] H. A. Lorentz, Ann. Phys. **248**, 127 (1881).
[42] C. L. Brooks, J. Solution Chem. **18**, 99 (1989).
[43] N. Khalil, C. López, and E. Hernández-García, J. Stat. Mech.: Theory Expt. (2017) 063505.
[44] L. Edelstein-Keshet, *Mathematical Models in Biology* (Society for Industrial and Applied Mathematics, Philadelphia, 2005).
[45] D. Levis and L. Berthier, Europhys. Lett. **111**, 60006 (2015).
[46] J. Palacci, C. Cottin-Bizonne, C. Ybert, and L. Bocquet, Phys. Rev. Lett. **105**, 088304 (2010).